Soft Matter

PAPER

View Article Online
View Journal | View Issue

Cite this: *Soft Matter*, 2017, 13, 2054

Clogging transition induced by self filtration in a slit pore†

B. Dersoir,[a] A. B. Schofield[b] and H. Tabuteau*[a]

Received 21st November 2016,
Accepted 13th February 2017

DOI: 10.1039/c6sm02605b

rsc.li/soft-matter-journal

Particles that flow through porous environments like soils, inside a filter or within our arteries, often lead to pore clogging. Even though tremendous efforts have been made in analysing this to circumvent this issue, the clog formation and its dynamics remain poorly understood. Coupling two experimental techniques, we elucidate the clogging mechanism at the particle scale of a slit pore with its height slightly larger than the particle diameter. We identify all the particle deposition modes during the clog formation and accurately predict the corresponding deposition rate. We show how the geometrical features of the pores and the competition between deposition modes can profoundly change the clog morphology. We find that the direct capture of particles by the pore wall is rather limited. The clog formation is more closely related to the short range hydrodynamic interaction between flowing particles and those which are already immobilized within the pore. Finally we demonstrate that all the clogging regimes can be gathered on a single phase diagram based on the flow conditions and the filter design.

1. Introduction

The transport, deposition and detachment of (bio)colloidal particles within porous networks often lead to progressive fouling or clogging. This issue occurs under various industrial conditions including all filtration steps,[1] heat exchanges,[2] oil recovery,[3] inkjet printing[4] or catalysis.[5] In natural environments, infiltration of water containing organic and inorganic solids (clay and silt particles, algae cells, and microorganisms) clogs soil pores[6] and river beds,[7] while the dissolution and precipitation of minerals alters the porous structure of rocks over time.[8] The human body is also affected by such issues when the buildup of plaques (fatty substance and cellular wastes) narrows arteries, up to the complete blocking of blood flow.[9] The visualization of the particle transport at the pore scale within model porous structures has allowed elucidation of all the relevant physical parameters related to the progressive clog formation.[10] These previous works have shown that a pore gets clogged when a fixed number of colloidal particles, N^*, have passed through it.[11–13] In a previous paper[12] we reported that particles first get captured at the surface of the pore wall in the vicinity of the entrance to the constriction/pore. Thereafter, various aggregates are formed on top of this first layer of particles. They grow until they merge and eventually clog the pore. In the case of a polydisperse colloidal suspension, the aggregates first grow until the remaining pore cross section is blocked by larger particles.[14,15] However, this work does not provide any indication of the dynamics of the overall clogging process at the particle scale. In particular, we still do not know (i) how the self-filtration occurs, *i.e.*, do the particles already captured help or prevent the deposition of new particles that enter the remaining pore space and (ii) what are the features of the aggregates such as their growth rate, mean internal volume fraction and their stability under flow ?

In this work we study the progressive obstruction of a pore at the particle scale in order to characterize the self-filtration process and its impact on the dynamics of pore clogging. We flow dilute and monodisperse colloidal suspensions in a very simple geometry, a slit pore with its height H slightly larger than the particle diameter D. We combine fast confocal imaging and streak velocity techniques to provide the dynamics of the particle capture within the pore and the capture rate. We also determine the different steps of the filtration process, from the particle capture by the pore wall up to the final pore blocking. We show that even under the conditions of very high confinement the filtration of suspended solids exhibits a rich variety of features, depending on the pore geometry, the flow conditions and also the immobilized particles within the pore.

2. Choice of the pore geometry and experimental conditions

Previously we considered the clogging of pore/constriction with a square cross section[12] (Fig. 1A, top) for various confinements, $1.5D < W < 10$, with W and D the width of the pore and the

[a] *IPR Université Rennes 1UMR CNRS 6251, Milieux Divisés, 263 avenue du Gal Leclerc, Rennes, France. E-mail: herve.tabuteau@univ-rennes1.fr*
[b] *School of Physics and Astronomy, The University of Edinburgh, The James Clerk Maxwell Building, The King's Buildings, Mayfield Road, Edinburgh, UK*

† Electronic supplementary information (ESI) available. See DOI: 10.1039/c6sm02605b

particle diameter, respectively. In this pore geometry the first step of the clogging formation corresponds to particle capture by the two lateral walls at the entrance of the pore (Fig. 1A, bottom). There is a physical interception of the particles by these walls. Particles come close enough to the pore surface and fall in the attractive part of the DLVO potential between the particle and the pore surface. In the present study we focus on the clogging dynamics in very high confinement, with the smallest pore dimension slightly larger than the particle diameter. In this case particle capture by the pore surface is supposed to be the main mechanism responsible for pore clogging. We decide to work with a network of elongated pores rather than square or circular ones. This type of design has the same selectivity as other geometries but a lower flux decline during fouling.[16,17] We first made this type of pore using single step lithography, *i.e.* we spin coat only one layer of photoresist with a height H, which is larger than the pore width W (Fig. 1B, top). In addition, we decided to study particle capture by only one side of the pore and in this case we used an asymmetric slotted pore. However, we observed that there are still two captures modes, one on each lateral wall (Fig. 1B, bottom), with particle deposition on the flat wall being less important than on the curved one. Ideally, we would have liked a high aspect ratio between the width and the pore height, *i.e.* W/H lower than 0.01, in order to have only one parabolic velocity profile in the flow direction, perpendicular to the pore height. In such a case, the features of the particle deposition are the same whatever the height of the particle just upstream from the pore entrance. However, it is rather difficult to make such a high aspect ratio channel as keeping the lateral walls vertical is problematic.

Most of the time the pore width is not the same at the top and the bottom. Moreover, using SU8 photoresist, narrow and high structures in our elongated pores, are fragile and easily bend due to capillarity during the final cleaning step of the lithography process and this prevents the PDMS from forming a suitable mold.[18–20] We had to restrict ourselves to aspect ratios higher than 0.25 in order to get vertical and stable walls, which is far from what we would have liked. By using two layer lithography, we found an alternative technique which better met all our requirements (Fig. 1C, top). We first made a thin layer of negative photoresist (SU8 2010) with a height H that corresponds to the pores height in the central part of the device (Fig. S1, ESI†). In the second step, we increased the thickness of the main channel on both sides of the slotted pore, called the reservoir zone (Fig. 1C, top), up to a height H_R. We did this by adding and aligning a second layer of photoresist. PDMS is then poured on the photoresist, cured and sealed onto a PDMS coated glass cover slip. The central part of the new design consists of a series of parallel slotted pores with a width W and

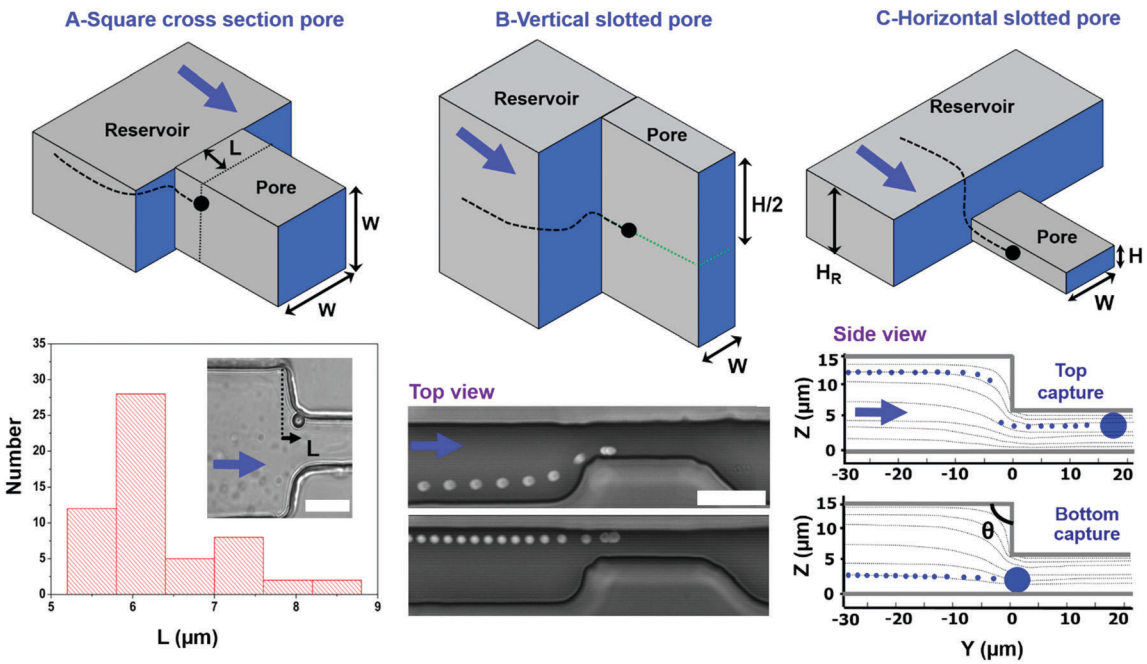

Fig. 1 Top – various geometries of the pore. We used a single layer lithography process to make the square cross section[12] (A) and the vertical slotted pore (B) and a two-layer process for the horizontal slotted pore (C). W, H and H_R correspond respectively to the pore width, the pore height and the reservoir height. Bottom – (A) 6 μm polystyrene diameter particles flow through a pore with W = 24 μm. The first deposited particles are captured by the pore lateral walls at a distance L from the pore entrance (inset), with a broad distribution (graph). Scale bar = 24 μm. (B) 1.8 μm PMMA particles flowing through an asymmetric constriction (vertical slotted pore) with W = 5 μm and H = 20 μm. We image the particles' motion prior to their capture with a high-speed camera (8000 frames per second) at the highest velocity position which is at the middle of the pore ($H/2$). Particles are either captured by the lateral flat wall (bottom image) or by the curved wall (top image). Scale bar = 20 μm. (C) Horizontal slotted pore. θ is the angle between the wall at the entrance of the pore and the horizontal top wall of the reservoir. In this case there are also two types of particle capture, the top capture (top image) and the bottom one (bottom image). The small (grey) dots are the fluid trajectory determined with COMSOL while the bigger (blue) dots are the trajectory of the particle obtained using the streak velocimetry technique. The blue arrow on each image points to the flow direction.

separated by a distance W_R between adjacent pores (Fig. S1 and S10, inset, ESI†). This gives us horizontal slotted pores rather than vertical ones. Particle capture remains the same in both geometries, but in the new one particles are mainly captured by the horizontal walls rather than by the lateral ones as long as the pore width W is far greater than the pore height H. Indeed, we found that there are also two capture modes (Fig. 1C, bottom), particles are either captured by the top or the bottom horizontal pore wall. In the former case which is also the most frequent event, particles are intercepted by the pore roof as they enter (Fig. 1C, top capture) while in the latter case, due to the asymmetry of the pore, particles follow the fluid flow streamlines until they touch the bottom horizontal wall (Fig. 1C, bottom capture). We used various height ratios H_R/H, between 1.7 and 8 and observed qualitatively the same results for all arrangements, *i.e.*, particles are captured at the pore entrance. We choose $H_R/H \sim 3$, H_R being between 13 and 21 μm while H is between 4.6 and 7 μm, since this ratio enables us to get sharp images of all the particles along the reservoir height with an ×40 objective lens, which is an important requirement for the determination of the particle altitude in various parts of the filter described below. In addition, we have a very high aspect ratio between the width and height of the reservoir zone, between 5×10^{-3} and 8×10^{-3}, so we can consider that we have only a parabolic flow profile along the reservoir height. We try to have an angle θ at the pore entrance (Fig. 1C, bottom) equal to 90 degrees. However, it is difficult to obtain this precise value since it is linked to the time of UV exposure of the SU8 master, and θ lies between 97 and 120 degrees for the different devices used. The roundness of the pore entrance does not seem to change drastically the position of the particles captured downstream in the pore. We previously worked with round corners and the particles get captured mainly on the curved part of the pore entrance, just before the straight part of the pore[12] (Fig. 1A, bottom). In the present study, the corners are straighter and particles still deposit near the entrance of the pore in the slotted horizontal pore. However, the deposition length from the pore entrance is larger since it can reach 4D (Fig. S2, ESI†), while it was much shorter in the former case, around 2D.

We have synthetized 4.0 ± 0.1 μm fluorescent PMMA particles by following the methods described in the paper of Shen *et al.*[22] These particles are monodisperse (CV = 2.5%) and are dyed with NBD (4-chloro-7-nitrobenz-2-oxa-1,3-diazote) which is excited at 488 nm and has a maximum emission at 525 nm. PVP chains that bear negative charges stabilize them against aggregation. The resulting zeta potential is equal to 70 mV. We worked with iso-dense suspension, *i.e.* the density of the liquid is the same that of the colloidal particles, by using a mixture of water (33% by weight), urea (37%) and glycerol (30%). We flow dilute suspensions though a microfluidic filter-like device (Fig. S1, ESI†) by imposing a constant pressure gradient across the microchannel thanks to precise pressure controllers (Elveflow and Fluigent). Particles coming from the reservoir zone flow through the pore/constriction, where the pore height is between 1.1 and 1.75D (Fig. 1A). We work with Re number smaller than 10^{-4} and the Pe number between 1 and 100. We used a high speed confocal microscope (VT-Infinity III, Visitech) to determine precisely (50 nm after image analysis) the position of the immobile particles within the pores (four to ten) during the filtration experiment. The images were analyzed with IDL (Interactive Data Language) and Matlab. Each pore is imaged every 30 s and the volume fraction of the injected suspension is between 10^{-6} and 10^{-4}, which ensures that no more than one or two particles at most deposit inside the pore between two consecutive acquired images, irrespective of the flow conditions. We do not observe, over the range of pressures used any detectable motion of the captured particles once they become immobile. Actually, only at the very highest pressures do a few particles move and this is over distances smaller than 1–2 μm during the entire experiment which lasts typically around 40 minutes. Experiments stop when half of the pores are clogged. It is worth noting that as the pore get clogged the probability to capture a particle by the wall does not decrease,[21] even though we worked with an imposed pressure. Actually, even when a pore is completely clogged the increase of the resulting hydrodynamic resistance remains pretty small. In the same way, the clogging of one pore does not change significantly the flow conditions in the adjacent pores. By knowing (i) the velocity in the reservoir zone of a particle about to be captured and (ii) by which wall, top or bottom, this particle is eventually captured, we can easily determine the particle altitude just upstream of the pore entrance.[21] We use this technique, called thereafter Particle Streak Velocimetry, to obtain the particle trajectories before their capture as shown in the bottom part of Fig. 1C. The principle of this technique involves the imaging of moving particles over large exposure time resulting in a blurred motion of the particles (Fig. 2A). The mean particle velocity is simply equal to the length of the particle trajectory or streak over the exposure time. A more detailed description of this technique is provided in another paper.[21]

3. The line to invasion clog transition

We first study the clogging dynamics for various flow rates Q, with a pore width W = 80 μm and a distance between adjacent pores W_R = 320 μm. Images of a pore at the end of the clogging process obtained for different Q values are shown in Fig. 2A. As expected, particles stop at the most confined space, they are captured by one of the horizontal walls at the pore entrance. All the deposited particles form a line-shaped clog (Fig. 2A-1) and then called hereafter the line regime. This behavior remains the same for $Q < 3$ μl min^{-1}, the average position of the clog front from the pore entrance, L, increasing slowly with Q (Fig. 2A-2 and B). Above a critical rate, Q_c, there is a second clogging regime called the invasion regime. In this region, the particles deposit further down the pore (Fig. 2A-3) with L increasing rapidly with Q until it levels off and becomes roughly equal to W, the pore width (Fig. 2B). The number of particles that have to pass through the pore prior clogging, N^*, follows almost the same evolution as that of the clog front L with Q (Fig. 2C), but with a sharper increase above Q_c. In order to

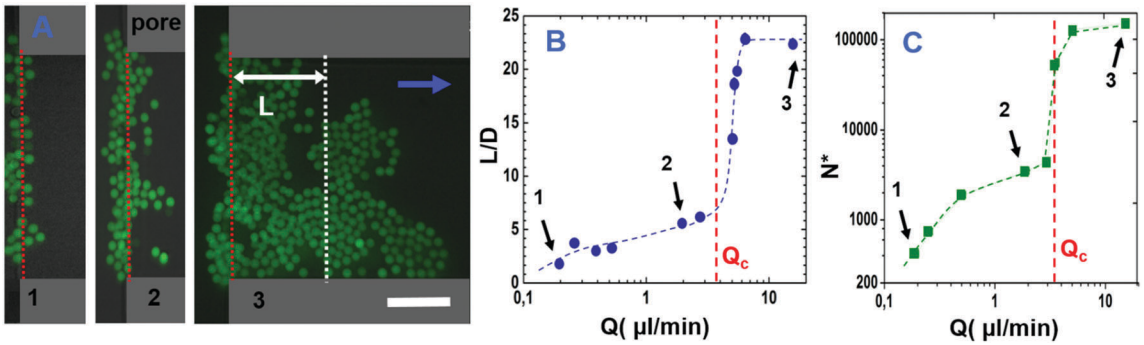

Fig. 2 (A) Clog morphology for various flow rates (0.2, 2 and 18 µl min^{-1} from left to right) within a pore of width W = 80 µm. Scale bar = 20 µm. The two grey rectangles and the dotted line correspond to the lateral walls of the pore and to the pore entrance, respectively. In image 3, we define the average position of the clog front L. Variation of the average clog length inside the pore, L, rescaled by D (B), and the average total number of particles N^* that pass through the pore prior clogging (C) with the flow rate. The vertical dashed lines correspond to the critical flow rate Q_c. The number 1 to 3 in plots B and C correspond to the image number. The blue arrows give the flow direction.

unravel the mechanisms behind this transition between these two clogging regimes we first determine the different deposition modes of particles that lead to the clog formation.

As mentioned earlier, particles are intercepted by one of the two horizontal pore walls; which is what we call direct capture. We found that particles get captured by the walls only near the pore entrance for all flow rates examined. The average deposition distance from the pore entrance, Y, increases with the flow rate, with a maximum value not greater than $4D$ (Fig. S2, ESI†). As in a typical filtration experiment, we define the features of the particle capture by the pore wall. More specifically, we define the capture zone as the range of altitude upstream in the reservoir, where the particles follow the fluid streamlines that are horizontal and from which all the particles that are eventually captured by the pore walls come from (Fig. S3A, ESI†).[23] Thanks to streak image analysis,[21] we can track a particle coming from this capture zone up to its stationary position within the pore. In this way, we determine the width, W_{capt}, and the center, Z_{capt}, of the capture zone in the reservoir (Fig. 3A, inset), and also the altitude and the position from the pore entrance of the immobile particles. The capture zone, is determined far enough upstream of the pore entrance, where the particle streamlines remain horizontal, 30–50 µm from the entrance, (Fig. 1C, bottom). The evolution of the position of the center, Z_{capt}, and the width, W_{capt}, of the capture zone with the flow rate for the direct capture mode are shown in Fig. S3B and D in the ESI.†

In this section we focus on the particles captured by the top wall, which is the main capture zone (Fig. S3A, ESI†). As the

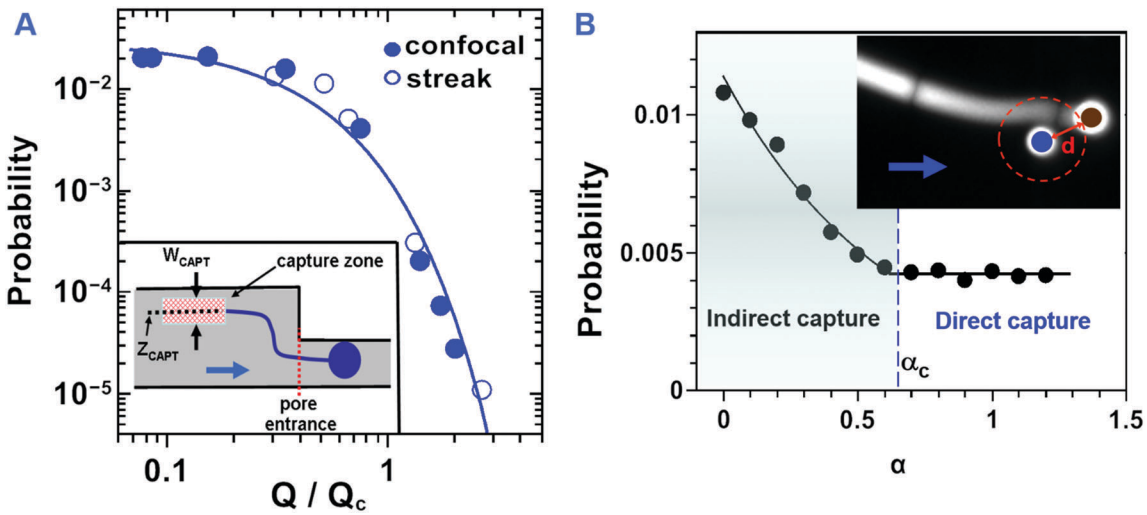

Fig. 3 (A) Evolution of the probability of the direct capture mode with the rescaled flow rate, obtained with the confocal (full symbols) and the particle streak velocimetry (open symbols). The line is an exponential fit of the data coming from the confocal microscopy: $P \sim 0.03.\ \exp(-3.12Q/Q_c)$. Inset: Definition of the capture zone in the reservoir zone with its width W_{capt} and its centre position Z_{capt} in a side view of the pore entrance. (B) Probability to capture a particle at a rescaled distance α of the nearest particles already deposited inside the pore, for Q = 0.3 µl min^{-1}. The rescaled distance is equal to d/D, with d the distance surface to surface between the two particles and D the particle diameter (inset). α_C corresponds to the rescaled distance beyond which the immobile particle does not influence the deposition of the others. Inset: Streak image of particle capture (blue) near an immobile one (brown). The arrow points to the flow direction.

flow rate increases, Z_{capt} gets closer to the pore wall and W_{capt} decreases rapidly down to 0.15μm for $Q = 2.7Q_c$ (Fig. S3D, ESI†). This leveling-off is an artifact related to the limit of our measurement accuracy on the z-position (±0.15 μm). Therefore, for high flow rates, for $Q > Q_c$, particles eventually intercepted are already very close to the wall far upstream of the pore entrance and the density within the capture zone starts to decreases (Fig. S3C, ESI†). The probability of capture, P is directly linked to the width of the capture zone within the reservoir and the particle density over the whole height of the reservoir:[11,21]

$$P = (Q_{capt}/Q_{total})\cdot(N_{capt}/N_{total}) = (W_{capt}\cdot V_{capt})/(H_R/V_{total})\cdot(N_{capt}/N_{total})$$

where, V_{capt} and V_{total} are respectively the mean velocities in the capture zone and in the overall height of the reservoir, H_R is the reservoir height, N_{capt} and N_{total} are the number of particle in the capture zone and the total number across the reservoir height, respectively. The density of particles, corresponding to the last ratio of this expression, is almost constant and then decreases for $Q > 1.8Q_c$ (Fig. S3C, ESI†). We found a good agreement between the probability P we got from the confocal measurements (plain symbols in Fig. 3A), and the one from the particle streak analysis (open symbols). P decreases continuously in an exponential manner over the Q range we used. This behavior is mainly due to the evolution of W_{capt} with the flow rate which also undergoes an exponential decay (Fig. S3D, ESI†).

At first glance, the different features of the direct capture mode are sufficient to explain the first clogging regime, the line regime. The small decrease of P with the flow rate, can correspond to the slight increase of N^* with Q. In addition, there is also a smooth increase in the distance of particle deposition from the entrance with Q (Fig. S2, ESI†), the capture of the particles still being located near the pore entrance, as observed for the clog length in Fig. 2B. In this view, particles are intercepted one after the other by the pore walls, forming progressively a line until the pore is completely blocked. However, direct capture cannot explain either the clogging transition, since there is no abrupt variation of P near the critical flow rate Q_c, nor the pore invasion. Indeed, this invasion process due to direct capture is rather limited since most of the particles are captured at a distance smaller than $4D$ from the pore entrance, even at the highest flow rates (Fig. S2, ESI†). As this capture distance is much smaller than the value of clog length L in the invasion regime ($\sim 23D$) we can conclude that there are other capture modes involved in the clogging dynamics, at least in the invasion regime. Thereafter, we would like to define these other modes using simple criteria still based on the distance between immobile particles in the pore. Since we study the clogging dynamics mainly from data obtained from confocal measurements the analysis of this gives us the precise position of the particle center but does not give us access to the motion of the particles prior to their capture. Another capture mode emerges if we remember that the direct capture involves only a flowing particle and one of the pore walls. Thus static particles inside the pore are not supposed to partake in the direct capture mode. However, as the pore get progressively clogged the deposition of a particle in the vicinity of immobile ones becomes more likely and then potential interaction between them may occur. To define the influence of static particles on the capture probability we study the dependency of the capture probability with the rescaled distance $\alpha = d/D$ between a freshly deposited particle and its closest immobile neighbor, with the distance d being between the two particles' surfaces (Fig. 3B, inset). For $\alpha > \alpha_C$, the probability to capture a new particle by the pore wall is constant (Fig. 3B), which corresponds to the direct capture, since there is no influence from the immobile particles. But, for $\alpha < \alpha_C$ this probability increases as α becomes smaller.

Thus, an immobile particle inside the pore modifies somehow the trajectory of others that flow in its close vicinity. For $\alpha < \alpha_C$ there is some binary hydrodynamic interactions (HI) between the flowing particle and the immobile one that increases the capture probability. In the following, if the HI lead to particle capture near an immobile one at a distance smaller than α_C, we call it aggregation since α_C is always smaller than 1, irrespective of the flow rate. This corresponds to a distance between the surface of the two particles smaller than D (Fig. 4B and C) and in such a case no other particle can flow in between them. Actually, this kind of particle couple forms an effective aggregate, a doublet, since the two particles touch one of the walls but are not themselves in contact. It is worth mentioning that the aggregation mode relies only on single binary HI between a particle that enters the pore and a static one. However, a flowing particle may undergone more complex HI, which involve more than two particles/aggregates and help it come closer to a wall and eventually get captured by the pore walls at a distance α greater than α_C. For instance, a mobile particle can either come across successive particle/aggregates (Fig. 4D and E) or flow between two aggregates/particles (Fig. 4F) before being captured by the pore walls. Thereafter, we call this third capture mode indirect deposition. It is worth noting that in this mode the distance α is greater than α_C, even though HI are mainly responsible for the particle capture. Actually, we suppose that a particle captured by this mode has flowed near particles or aggregates at a rescaled distance β, measured from particle surface to particle surface, which is smaller than α_C, since it is the threshold distance below which binary HI occurs and modifies the particles' trajectory (Fig. 4, indirect deposition-left). In the same way, when a particle is flowing between two aggregates (or particles) the distance δ between the surfaces of those aggregates is smaller than $2\alpha_C$. (Fig. 4, indirect deposition-right). This length criterion ensures that the particle flows at a distance $\beta < \alpha_C$ from one of the two surfaces, as well. In our classification we do not take into consideration the size and the orientations of the aggregates with respect to the flow direction, within which the flowing particles pass through. To sum up we have two modes of particles capture by the pore walls, direct or indirect (aggregation and indirect deposition) that we put together in Fig. 4.

In the following, we focus on the overall clog formation for various flow rates using a colour code as defined in Fig. 4 for each mode of particle capture (Fig. 5). In the ''line regime'' and for the lowest flow rate ($Q/Q_c = 0.076$), we mostly observe pore clogging by direct capture of particles (blue) along the pore entrance (Fig. 5A-1–2). In a lesser extent the particle deposition

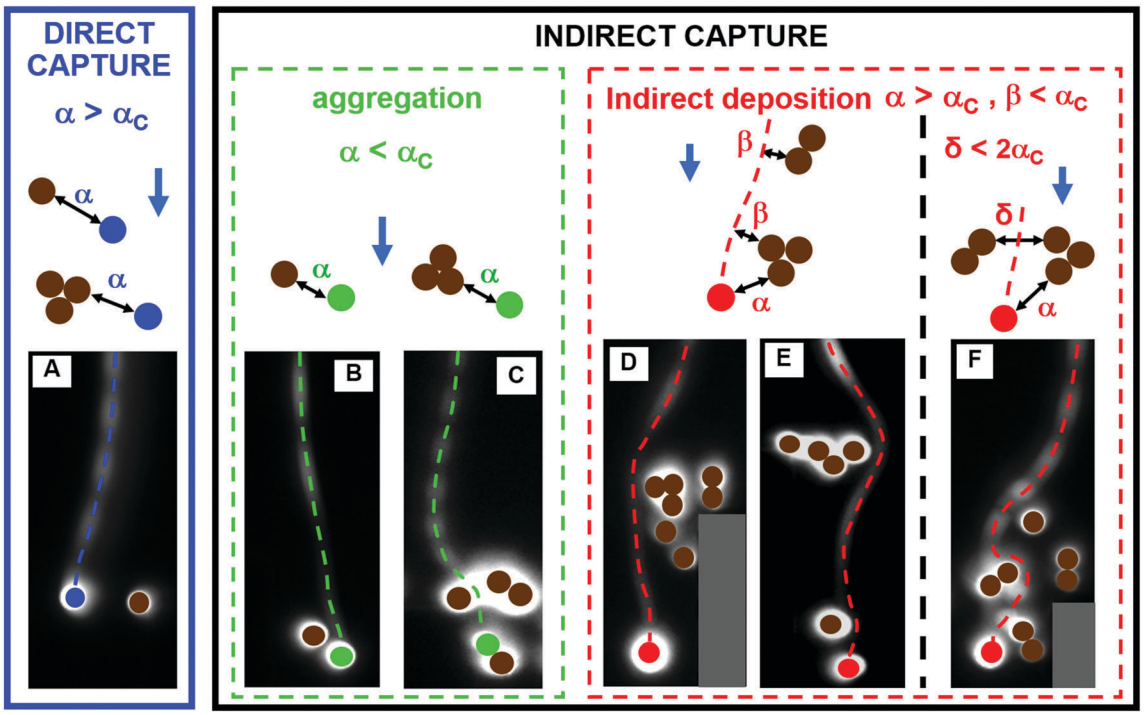

Fig. 4 Different capture mechanisms of particles by the horizontal pore walls. For all the modes the schematics correspond to the final position of a particle just after its capture, relative to other immobile particles. The new deposited particles are in blue (direct capture in image A), green (aggregate in image B and C) or red (indirect deposition in images D to F) while those already captured in the pore. The rescaled distance α is equal to d/D, with d the distance surface to surface between the freshly deposited particles and their closest neighbor which, may already, belong to an aggregate. In the indirect deposition the rescaled distances β and δ correspond respectively to the minimum distance between a flowing particle and an obstacle (particle or aggregate) and the distance between two aggregates (or particles) a particle has to go through. The grey rectangles in images D and F correspond to the lateral wall of the pore.

related to the indirect capture also increases (Fig. 5A-2–4). Almost all these particles (green) stop really close or in contact with an immobile one at the pore entrance. The deposition of the red ones, corresponding to the indirect deposition, remains rather limited and most of the time, they show up near the end of the clog formation (Fig. 5A-3–6). Interestingly, we consider that in image 6 the pore is completely clogged even though not all the particles within the clog are in contact. Actually, in such high confinement two particles that belong to the clog have to be close enough (at a distance smaller than D) to not allow others to flow between them. We may also note that some deposited particles do not partake in the clog (orange line in Fig. 5A-6). For a higher flow rate closer to the transition ($Q/Q_c = 0.76$), most of the features are the same, but we observe that, on average, particles are deposited further down the pore, (Fig. 5B). In addition, the number of indirect capture events becomes higher than those of direct capture.

At the end the process, the shape of the clog is still a line but this is more tortuous than for lower flow rates (Fig. 5B-6) and the number of deposited particles downstream of the clog front, *i.e.*, that do not belong to the clog, also increases. Finally, in the invasion regime and well above Q_c ($Q/Q_c = 2.33$), the situation is quite different (Fig. 5C-1–3). Once a particle deposits anywhere at the pore entrance (blue) an aggregate (made of green particles) rapidly grows. The deposition by direct capture stops rather rapidly in the clogging process (maximum number of blue particles is reached in Fig. 5C-4). The pore filling by particles relies mainly on the indirect capture mode. Particles that encounter an aggregate near the pore entrance or flow through particle assemblies (red ones) deposit further downstream inside the pore. As before, as soon as one of those particles deposits within the pore many particles (green ones) are captured in its vicinity (Fig. 5C-2–5).

Aggregates of particles formed in this way far from the pore entrance in their turn, help other individuals (red ones) to deposit further downstream and new aggregates to grow there and so on up to pore clogging (Fig. 5C-5–10). At the end, the clog front exhibits a complex shape (orange line in Fig. 5C-10) and once again lots of deposited particles do not belong to the front (Fig. 5C-10). These conclusions on the role of the different capture modes on the clog formation are further supported by the evolution of the average deposition probability of each capture mode with the flow rate (Fig. 6). We clearly distinguish two regimes. Up to $Q = 0.6Q_c$ the direct capture mode and the aggregation mechanism decreases in the same manner with Q; the probability of the direct capture being slightly greater. The probability of the indirect deposition remains the smallest within this range of Q. Around the transition ($0.7Q_c < Q < 1.3Q_c$), the probability of the direct capture mode and the indirect deposition are almost identical, both decreasing with Q faster than the aggregation probability. For higher flow rate, from $Q \approx 1.3Q_c$, the indirect capture modes largely dominate over the direct one.

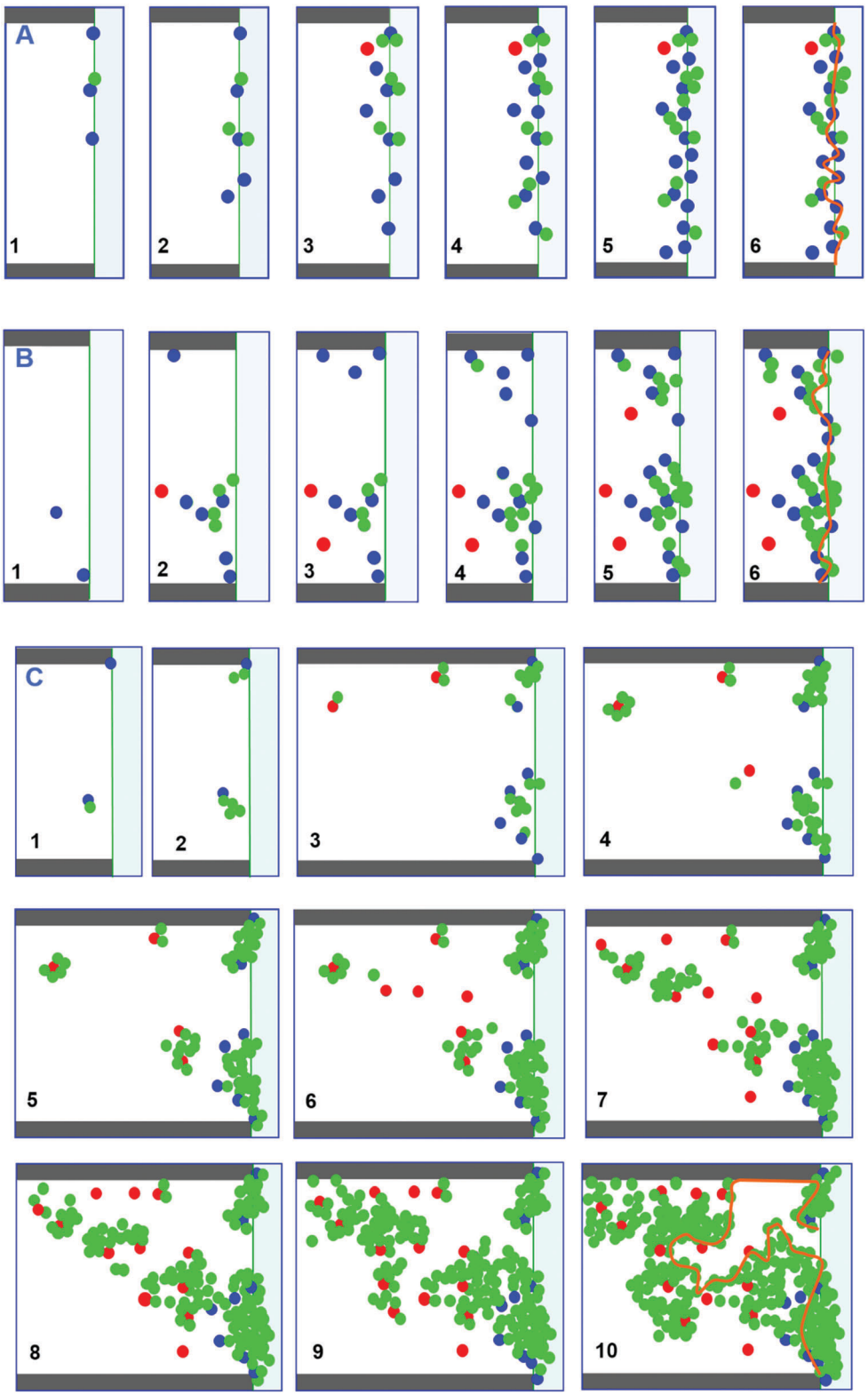

Fig. 5 Consecutives images of the clog building up for $0.076Q/Q_c$ (A), $0.76Q/Q_c$ (B) and $2.33Q/Q_c$ (C). The pore width is 80 μm and the color code for the particles is the same as the one defined in Fig. 4. The vertical green lines and the tortuous orange lines correspond to the pore entrance and to the clog front respectively. The flow is directed towards the left.

Actually, the aggregation probability is ten times greater than the indirect deposition probability, which in turn is one order of magnitude larger than that for direct capture. This simply means that aggregates grow faster than the isolate particles

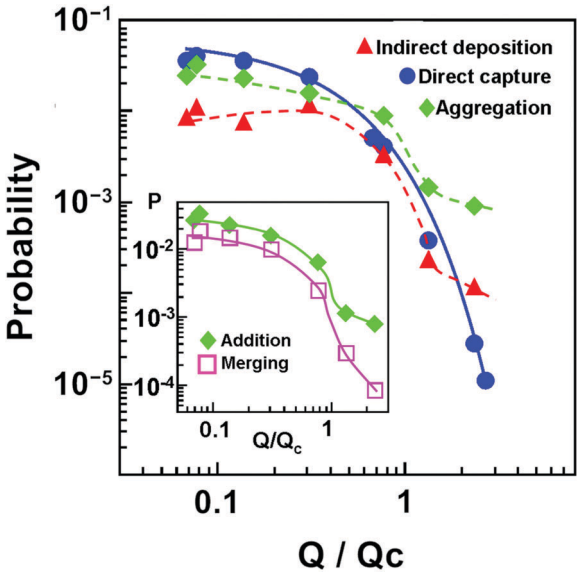

Fig. 6 Variation of the probability for each deposition mechanism, averaged over the entire clogging experiment, with the rescaled flow rate. The continuous line is an exponential fit of the data ($P = 0.06\exp(-3.12Q/Q_c)$) while the dashed lines are just guides to the eye. Inset: Probability for the two aggregation modes (aggregation by particle addition or merging).

deposit either at the pore entrance or further downstream. There are two modes of aggregate growth under flow, irrespective of Q. A particle either deposits near a particle/aggregate (addition mode, Fig. 4B and 7B2), with $\alpha < \alpha_C$, or get captured in between two aggregates/particles, forming in this way a bigger aggregate (merging mode, Fig. 7B3–5). The competition between these two growth modes depends on the flow rate (Fig. 6, inset).

In the line regime, for $Q < Q_c$ most of the particles (60 to 70%) deposit near the pore entrance, at a distance such that $\alpha > \alpha_C$ (Fig. 7A, top row). Therefore, there is a direct physical interception of these particles by the pore walls that is not influenced by the presence of any immobile particles. Also, these particles do not partake in aggregate growth, as earlier defined. Aggregates first grow by particle addition, in a rather limited fashion (Fig. 7C), and once triplets up to quintuplets are formed they can grow only by merging with another adjacent aggregate. A typical example of the growth of an aggregate in the line regime is shown on Fig. 7B (images 1 to 4). This aggregate growth is a two-steps process as long as $Q < 0.8Q_c$, and the probability related to the addition mode being roughly two times greater than that of the merging mode (Fig. 6, inset).

In the invasion regime, for $Q > Q_c$, the situation is reversed and most of the particles, between 60 and 70%, are deposited near a particle/aggregate with $\alpha < \alpha_C$ and therefore belong to an aggregate (Fig. 7A, left bottom corner). In this case, the aggregate growth, which is chiefly due to the addition mode (Fig. 6, inset), is much more important than before. The average

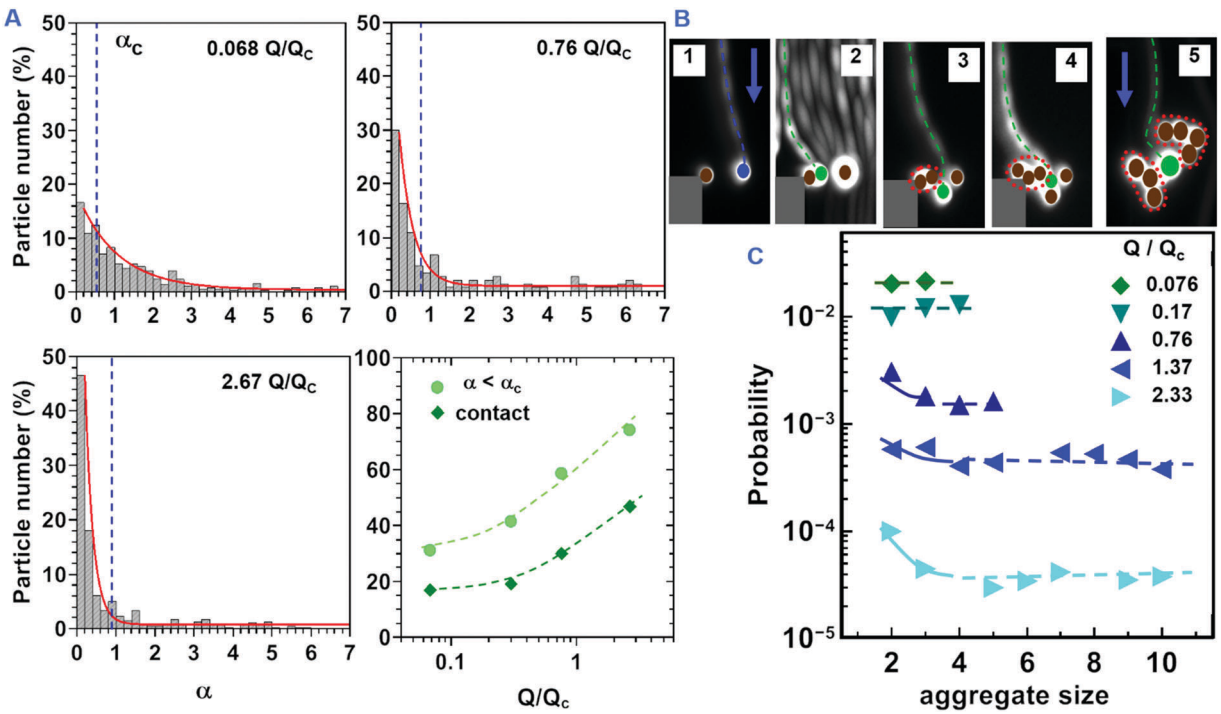

Fig. 7 (A) Histogram of the number of particles that are at a given distance α to their closest neighbour within the pore for various flow rates. The graph in the bottom right corner shows the evolution of the percentage of the total particle number that belong either to aggregates in which particles are not necessarily in contact (circles) or to aggregates where particles touch one another (diamonds). The vertical dashed lines (blue) and the continuous ones (red) correspond to the distances α_C and to exponential fits of the data. (B) Consecutive images of the growth of an aggregate from one side of the pore in the line regime. Image 5 corresponds to the merging of two adjacent aggregates (within dotted lines) when a particle comes and stops between them. Arrows point to the flow direction. (C) Variation of the probability to add a particle to an aggregate with a given size for various flow rates. The dashed lines correspond to the average probability for each flow rate.

number of particles per aggregate before adjacent aggregates merge is around twenty particles. Strikingly, the rate of aggregate growth for the addition mode and for a given Q does not change with the aggregate size (Fig. 7C). This is all the more surprising because all those aggregates have various shapes and their locations within the pore are different, especially in the invasion regime (see Fig. 5C). In addition, the aggregate growth is not modified when the different aggregates are close to each other, even if they are about to merge. All these aggregation features are really different to those obtained in advective DLA simulation in 2 d where fractal growth is observed,[24] and also in other experimental studies that used similar confinement conditions, *e.g.* with a ratio pore height/particle diameter equals to two, and where chain-like aggregates grow along the flow direction.[25,26] These observations suggest that the aggregate growth in our case depends mainly on the local properties around the aggregates, at the particle scale. The binary HI between particles situated at aggregate edges and one flowing, which is about to be captured, is solely involved in the growth of aggregates as can be seen on the movies M1 and M2 (ESI†) which were collected using high speed imaging. We observe that the probability to capture a particle at a distance d from another one that was just captured (Fig. S5, ESI†) decreases quite rapidly with increasing d. Beyond a particle diameter, $d > D$, this probability becomes constant and then we may suppose that the immobile particles do not modify the trajectory of the flowing ones.

The immobile particles play a role similar to that of a collector grain in a classical filter bed. When a flowing particle comes too close to a static one they cannot avoid the interception by this obstacle (movie M1 and M2). During this capture event a flowing particle comes into contact with the still one and then rotates around it until it gets blocked between this latter one and the horizontal wall (Fig. 8, inset for $Q > Q_c$).

From those various analyses we can explain why there is a transition from the line to the invasion regime as the flow rate increases. For low Q in the line regime, the direct interception of the particles by the pore walls, mostly by the top one (Fig. 8) is the main mode of particle capture. Almost all the particles are captured in this way near the pore entrance and form line-shaped clogs. The presence of particles already deposited within the pore does not modify significantly the capture of the following ones, which still deposit at the pore entrance. However, we observe that the repartition of the captured particle between the top and the bottom wall changes when Q becomes greater than Q_c. In the invasion regime the probability of observing a direct capture by the pore wall keeps decreasing and becomes smaller than the indirect capture due to the particles already immobilized inside the pore, which modify the trajectory of those flowing. We suppose that the hydrodynamic repulsion between the mobile and the immobile individuals is responsible to the particle capture within the pore.[27] For instance, a particle that flows along the bottom wall is pushed towards and captured by this wall when it encounters along its path an immobile particle that lies on the top wall. By symmetry, the particle capture by the top wall, due to immobile ones deposited on the bottom wall, is exactly the same. Therefore, there is an equal probability to deposit a particle within the pore either on the top or on the bottom pore surface. We observe that in the invasion regime there is equal repartition of the particle on both horizontal walls irrespective of the flow rate (Fig. 8). The growth of a large aggregate over time following this mode of particle capture in the invasion regime is shown in Fig. S4 in the ESI.†

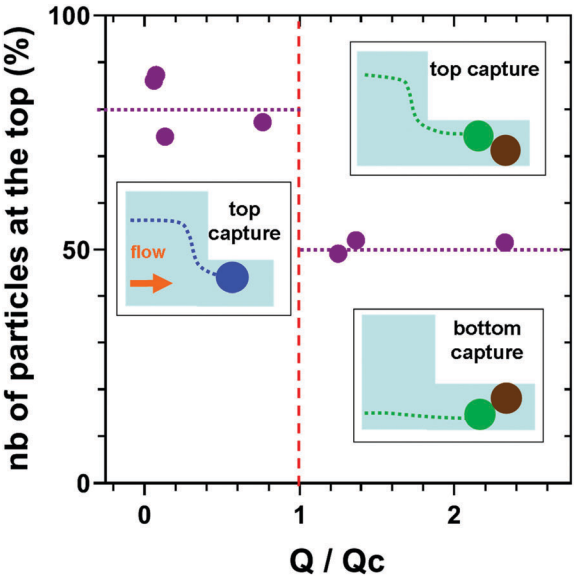

Fig. 8 Evolution of the percentage of particles captured by the top wall of the pore with the rescaled flow rate. Inset: For $Q < Q_c$, particles are mainly captured by the top wall while for $Q > Q_c$ they are captured between a particle and the opposite horizontal wall.

So far we have only studied a single geometrical configuration, the width of the pore W and the distance between adjacent pore W_R being fixed. To test the generality of our results, we experimented with various pore widths, W, distances between adjacent pores, W_R (Fig. 10A, inset), pore heights H and angles at the pore entrance θ. We first show that the value of Q_c and the variation of clog length L with flow rate are the same whatever the angle at the pore entrance, θ, and whatever the pore height, as long as $H < 1.75D$ (Fig. 9A). Indeed, the angle θ was varied from 95 to 120° when we use the smaller and the taller reservoir, respectively. Similar conclusions are drawn for the evolution of L with Q and the value of Q_c when we used different pore widths, keeping the ratio W_R/W fixed (Fig. 9B).

In addition, we observed that there is a linear variation in clog length with pore width for both clogging regimes, for a given ratio W_R/W and a fixed flow rate. In the line regime, the clog is still formed at the very entrance of the pore since there is a very small increase of L, around 1.5 μm, as the width of the pore is increased six fold (Fig. 9C, bottom). This increase is far more important in the invasion regime and we observe that $L \sim W$ (Fig. 9C, top). We found that there is significant variation in the features of the clogging transition when we use different width ratio W_R/W (Fig. 10B). When the pores are wider than the distance between adjacent pores, for instance for $W_R/W = 0.5$, the line regime spans over a wider Q range and the invasion

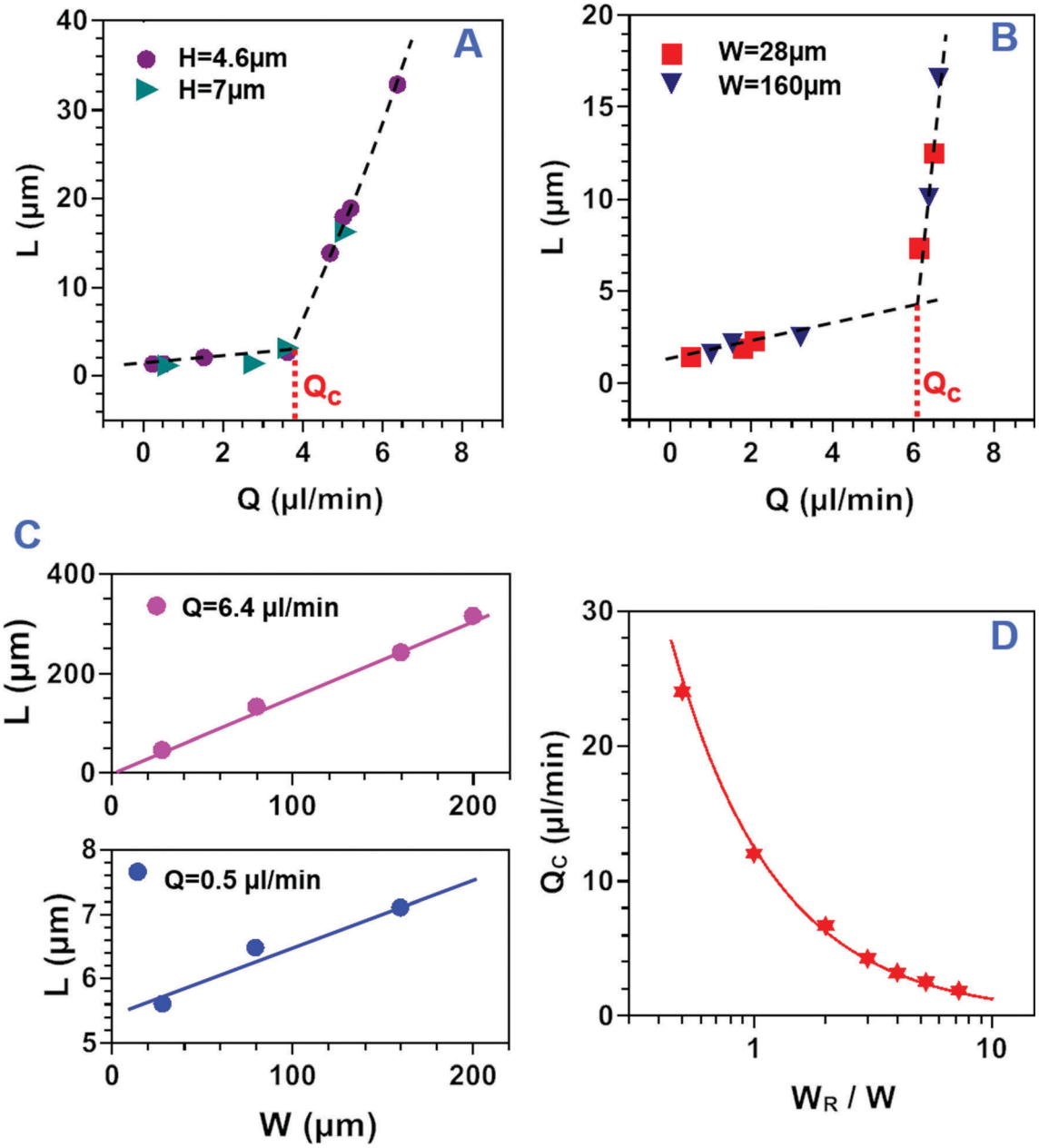

Fig. 9 Variation of clog length L with the flow rate Q for two pore heights (A) and two pore widths (B), keeping $W_R/W = 4$. The dashed lines are a guide for the eye and their crossing corresponds to the critical rate Q_c. (C) Clog length dependence with the pore width, corresponding to the line regime (bottom) and the invasion regime (top), with $W_R/W = 4$. The two lines are linear fits with slope 1.53 (blue) and 0.01 (magenta). (D) Evolution of Q_c with the ratio W_R/W. The continuous line is an inverse power law of the data.

regime starts for a higher critical rate. In this case, most of the particles are deposited near the pore entrance, irrespective of the flow rate (Fig. 10a and b). Even for $Q > Q_c$, the invasion of the pore with Q is slow and rather limited since the maximum value of L is not greater than $6.3D$, for the highest flow rate above which a clog cannot be formed anymore. In addition, only a few isolated particles are deposited past the clog front, further downstream in the pore. The situation is quite different when the distance between pores is larger than the pore width (see ratio $W_R/W = 4$ in Fig. 10B). Particles deposit all along the pore even in the line regime (Fig. 10c) and we go out of this regime for a smaller Q_c value than before. Moreover, the clog transition is much sharper with the length of the clog increasing more rapidly with Q in the invasion regime. Even though the clog is located at a distance $L \sim W$ in this regime, there are very large aggregates further downstream within the pore, even up to the pore exit (Fig. 10d).

We perform systematic experiments using various pore width ratios, from $W_R/W = 0.25$ up to 7, in order to determine more precisely the evolution of the features of pore invasion as the width ratio is altered. Instead of plotting the evolution of the value of the clog length with flow rate, as in Fig. 10B, we determine

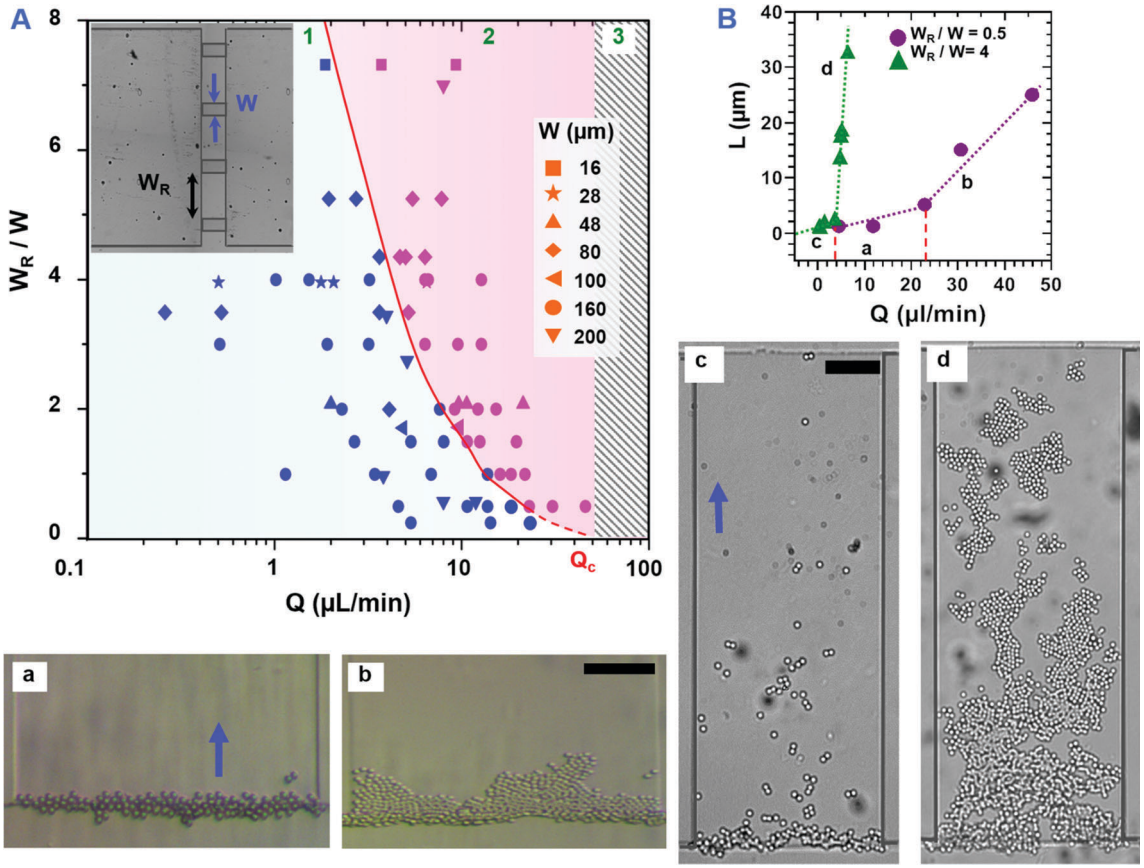

Fig. 10 (A) Clogging morphologies obtained for various combinations of the ratio W_R/W (see inset) and flow rates. There are three distinct zones (green labels). The lines regime (blue symbols) occur for low flow rates while the invasion one is observed at higher flow rates (magenta symbols). The red thick line is the frontier between the line and the invasion regime. Above $Q > 50$ µl min^{-1} (hatched zone) no particles deposit permanently within the pore. (B) Variation of L/D with Q for two ratio W_R/W. The critical rates correspond to the vertical red dotted lines. The letters a–b and c–d correspond respectively to clog images for $W_R/W = 0.5$ and $W_R/W = 4$ in the line and in the invasion regime, respectively. The arrows give the flow direction on the images. The pore width is equal to 160 µm and the scale bars on the images correspond to 40 µm.

for each data pair (W_R/W, Q) the morphology of the resulting clog, *i.e.* whether it is a line or invasion clog. To do so we have to define a criterion on the value of the clog length above which there is an invasion of the pore, irrespective of the width ratio. We have seen that the line regime relies mostly on the direct capture of particles by the pore walls; this deposition mode allowing the capture at a distance smaller than $4D$ on average, from the pore entrance. Therefore we choose the clog length that delimits the end of the line regime as equal to $4D$. This approach allows us to show that all the features of the pore clogging can be gathered in a single phase diagram which is shown in Fig. 10A. Surprisingly, this diagram tells us that whatever the value of W (16 to 200 µm) and W_R (40 µm up to 1.4 mm), for a given width ratio W_R/W, the transition between the two clog regimes always occurs for the same value of Q_c and the evolution of the clog length with Q is also identical (Fig. 10B). The first part of the diagram corresponds to the first clog morphology, the line-shaped regime (zone 1, blue symbols online in Fig. 10A) and this occurs when $L < 4D$, while the invasion regime is obtained for flow rates higher than Q_c (zone 2, magenta symbols) when $L > 4D$. Finally, in the third zone of the diagram for flow rates greater than 50 µl min^{-1}, there is almost no particle deposition and thus no clogging. In this last zone, the flow is strong enough so that it can detach a particle from the pore wall, *i.e.* to pull out the particle of the attractive part of the DLVO potential.[12] Hereafter we focus on the transition between the zone 1 and 2. We see that this clogging transition depends mainly on the width ratio W_R/W (red lines in Fig. 10A).

It is worth noting that the critical flow rate Q_c is inversely proportional to W_R/W (Fig. 9D) and for the smallest width ratio we studied, $W_R/W < 0.5$, the invasion regime starts for the highest critical rate, $Q_c \sim 24$ µl min^{-1}. We propose a simple explanation for this latter expression, based on the ratio between the numbers of particles that come from the central part of the reservoir over those coming from the sides of the pore N_{center}/N_{side} (Fig. S6A and B, ESI†). Indeed, we deduce from a simple conservation of volume argument and from the hypothesis that the distribution of the flowing particles is uniform across the main channel cross section, *i.e.*, perpendicular to the flow direction, that W/W_R is proportional to N_{center}/N_{side} and then $Q_c \sim N_{center}/N_{side}$. Therefore, the greater N_{side} the smaller is Q_c. This suggests that the arrival of particles within the pore by its sides enhances the pore invasion. The following arguments

support this hypothesis. For $W > W_R$ and $Q > Q_c$ direct capture of particles in the center zone occurs at a distance not greater than 4D in average (Fig. S2, ESI†). Rapidly thereafter a few individuals are captured in this way; aggregates grow and merge up to the pore clogging. There are very few depositions of isolated particles ahead of the clog front, further downstream within the pore, since the probability of the aggregate growth is much greater than that of indirect deposition (Fig. 6). Therefore, when most of the particles come from the center zone, *i.e.*, for $W > W_R$, the pore invasion is rather limited. On the other hand, we observe that for $Q > Q_c$ the direct capture of particles near the lateral walls of the pore occurs at a larger distance from the pore entrance (Fig. S6C, ESI†) than for the particle captured in the central zone, (Fig. S2, ESI†). This is due to the fact that the local shear rate is smaller near the lateral walls than in the center zone. Thus, the particles near the walls are less likely to be wiped out by the flow. In addition, the probability to capture a particle near the lateral walls increases with W_R, since there are more particles coming from the sides than for the center part. Consequently, the invasion of the pore starts for smaller Q_c when W_R increases, for a given pore width.

4. Discussion

We show that for whatever pore geometry employed, there is a line-to-invasion clog transition at a critical flow rate Q_c during which the evolution of clog length changes with the flow rate. These features of the clog transition, especially the value of Q_c, depend mainly on (i) the competition between two modes of particle capture by the pore walls and on (ii) the design of the pore entrance, especially on the width ratio W/W_R. A further extension of our work could focus on this latter point. Indeed, it would be interesting to decrease the width ratio towards zero and for this particular design, we would only need one long pore, with a step at the middle corresponding to a variation of height. If we extrapolate the inverse power law towards $W/W_R = 0$ in Fig. 9D and 10A (red dashed line) we end up with a critical flow rate equal to 50 μl min^{-1}, above the threshold at which the flow is able to detach particles from walls, *i.e.*, particles cannot be captured anymore by the pore walls. Therefore, in this geometry there is only one clogging regime, the line regime, which spans the broadest range of flow rates. In addition, the probability of particle capture and pore clogging would not change that much (by less than one order of magnitude) with Q for this design since it should correspond approximately to the slow decrease of the capture probability of the direct mode for $Q < Q_c$ in Fig. 6.

In this work we restrict ourselves to a high confinement regime with $1.1D < H < 2D$ but, obviously, decreasing the confinement and working with $H > 2D$ would be of great interest for many industrial applications. In particular, one would like to know if there exists a critical height H_c, above which particles are captured by the pore walls but no clogging can occur. As mentioned just above it is likely that a criterion based solely on the pore height o is insufficient to determine this, and we also need to consider the width ratio W/W_R. We think that if one works with a wide single channel, corresponding to $W/W_R = 0$, with a height step where the particle capture will take place, and a pore height $H > 4$–$5D$ pore clogging should not occur. For such a pore height, the top and bottom horizontal walls of the pore may be completely covered by particles but it is unlikely that a second layer of particles will build up on top of this monolayer. In particular, the indirect capture mode which is based on the repulsion of a flowing particle by an immobile one (Fig. 4, right panel), should not be effective to build this second layer for taller slotted pores. However, the accumulation on top of the first layer can be observed on the lateral/side walls of the channel and this may lead to pore clogging. Indeed, we show in a previous paper that the capture of flowing particles by other immobile ones inside the pore can occur only at the pore corners for a pore with a square or rectangular cross section and this accumulation process ends up with the pore clogging.[12] As far as the geometrical aspects are concerned the capture efficiency could be increase by using a symmetric pore instead of an asymmetric one. Indeed, if there is a step on the top and also on the bottom wall at the very entrance of the pore the capture probability of the direct mode will be simply doubled. Once again this is unlikely to change the features of the clogging transition. Other parameters more related to the particle could have a potential influence on these features, such as the particle's physical properties. We think that all the features of the two capture modes will remain the same when we change the particle size as long as we keep the same confinement ratio H/D, since the flow conditions will also be identical.

We performed experiments with dispersions of various ionic strength and found that the capture probability of the direct mode did not change.[21] This is not surprising since the pore walls are made of PDMS, which does not bear any surface charge. If we work with charged pore walls, these charges will prevent the particle capture for low flow rates, corresponding to Pe number smaller or close to unity. Therefore, charged walls will shorten the Q range of the line regime. Working with different particles, will also have an impact on the features of the clogging transitions, particularly on the value of Q_c. If we use for instance polystyrene (PS) rather than PMMA particles, since the Hamaker constant is greater in the PS case, the flow rate needed to detach the particles from the wall will be higher and so will be the value of Q_c. However, we think that changes in the adhesion properties will not significantly affect the direct capture mode. There will be marginal modifications to the deposition length of the particle from the pore entrance. Changing the nature of the pore wall, working with PMMA walls for instance, will have the same influence as changing the nature of the particle.

5. Conclusions

We provided a comprehensive study of the progressive clogging of a slit pore with its height slightly greater than the particle diameter. We have been able to do it only because we used two imaging techniques. The fast confocal set-up helps us to get enough statistics on the particle capture events and on their

3d positions within the pore, whereas the streak velocity technique allows us to capture the dynamics of the particle deposition. We showed that, depending on the flow conditions and the pore geometry, the clogging within a very confined space gives rise to unexpected phenomena, like the line-to-invasion clog transition. At low flow rates particles are mainly captured by the pore walls and form line-shaped clogs at the pore entrance while above a critical rate there is an invasion of the pore, the clog front being located far downstream inside the pore. This work demonstrates that self-filtration plays a central role in this second regime of clogging. We think that new strategies can be employed to enhance the performance of micro-filters if the features of the self-filtration process at the particle scale are better understood. Here, we focus on spherical particles, but our methodology can be extended to more complex suspensions, that contain either soft (droplets, capsules, cells and red blood cells) or anisotropic particles (clay, bacteria, virus, microfiber). In this work, we define all the mechanisms of particle deposition and how the competition between them leads to different clog morphologies. However, we do not address the hydrodynamics of the particle capture, directly or not, by the pore wall. Such studies could help to further understand the self-filtration process and also quantify the aggregate growth that leads to the pore clogging.

Acknowledgements

We would like to thank Jeffrey Morris for the reading of an early version of the manuscript. We acknowledge the support of the Agence Nationale de la Recherche (ANR) (ANR-12-JS09-0003) and the CNES (Collmat).

References

1 D. C. Mays and J. R. Hunt, *Environ. Sci. Technol.*, 2005, **39**, 577–584.
2 D. Kunii and J. M. Smith, *AIChE J.*, 1960, **6**, 71–78.
3 M. Tavakkoli, M. R. Grimes, X. Liu, C. K. Garcia, S. C. Correa, Q. J. Cox and F. M. Vargas, *Energy Fuels*, 2015, **29**, 2890–2900.
4 S. B. Fuller, E. J. Wilhelm and J. M. Jacobson, *J. Microelectromech. Syst.*, 2002, **11**, 54–60.
5 R. L. Hartman, J. R. Naber, N. Zaborenko, S. L. Buchwald and K. F. Jensen, *Org. Process Res. Dev.*, 2010, **14**, 1347–1357.
6 C. Mikutta, F. Lang and M. Kaupenjohann, *Soil Sci. Soc. Am. J.*, 2004, **68**, 1853–1862.
7 K. J. Rehg, A. I. Packman and J. Ren, *Hydrol. Processes*, 2005, **19**, 413–427.
8 C. Hilgers and J. L. Urai, *J. Struct. Geol.*, 2002, **24**, 1029–1043.
9 M. B. Rothberg, *Circ.: Cardiovasc. Qual. Outcomes*, 2013, **6**, 129–132.
10 E. Dressaire and A. Sauret, *Soft Matter*, 2017, **13**, 37–48.
11 H. M. Wyss, D. L. Blair, J. F. Morris, H. A. Stone and D. A. Weitz, *Phys. Rev. E: Stat., Nonlinear, Soft Matter Phys.*, 2006, **74**, 061402.
12 B. Dersoir, M. R. de, S. Vincent, M. Abkarian and H. Tabuteau, *Microfluid. Nanofluid.*, 2015, **19**, 953–961.
13 S. S. Massenburg, E. Amstad and D. A. Weitz, *Microfluid. Nanofluid.*, 2016, **20**, 94.
14 B. Mustin and B. Stoeber, *Microfluid. Nanofluid.*, 2010, **9**, 905–913.
15 A. Sauret, E. C. Barney, A. Perro, E. Villermaux, H. A. Stone and E. Dressaire, *Appl. Phys. Lett.*, 2014, **105**, 074101.
16 A. J. Bromley, R. G. Holdich and I. W. Cumming, *J. Membr. Sci.*, 2002, **196**, 27–37.
17 M. E. Warkiani, F. Wicaksana, A. G. Fane and H.-Q. Gong, *Microfluid. Nanofluid.*, 2015, **19**, 307–315.
18 T. Tanaka, M. Morigami and N. Atoda, *Jpn. J. Appl. Phys.*, 1993, **32**, 6059.
19 A. del Campo and C. Greiner, *J. Micromech. Microeng.*, 2007, **17**, R81.
20 K. Singh, J. R. Lister and D. Vella, *J. Fluid Mech.*, 2014, **745**, 621–646.
21 Dersoir *et al.*, 2016, submitted.
22 S. Shen, E. D. Sudol and M. S. El-Aasser, *J. Polym. Sci., Part A: Polym. Chem.*, 1993, **31**, 1393–1402.
23 A. Espinosa-Gayosso, M. Ghisalberti, G. N. Ivey and N. L. Jones, *J. Fluid Mech.*, 2012, **710**, 362–378.
24 B. Davidovitch, J. Choi and M. Z. Bazant, *Phys. Rev. Lett.*, 2005, **95**, 075504.
25 T. Gudipaty, M. T. Stamm, L. S. Cheung, L. Jiang and Y. Zohar, *Microfluid. Nanofluid.*, 2011, **10**, 661–669.
26 M. T. Stamm, T. Gudipaty, C. Rush, L. Jiang and Y. Zohar, *Microfluid. Nanofluid.*, 2011, **11**, 395–403.
27 G. C. Agbangla, E. Climent and P. Bacchin, *Comput. Fluids*, 2014, **94**, 69–83.

